APPLIED ORGANOMETALLIC CHEMISTRY
Appl. Organometal. Chem. 2001; **15**: 794–808
DOI: 10.1002/aoc.238

Phase equilibria of precursor-derived Si–(B–)C–N ceramics

Hans Jürgen Seifert,* Jianqiang Peng, Jerzy Golczewski and Fritz Aldinger
Max-Planck-Institut für Metallforschung und Institut für Nichtmetallische Anorganische Materialien, Universität Stuttgart, Pulvermetallurgisches Laboratorium, Heisenbergstraße 5, D-70569 Stuttgart, Germany

Phase equilibria and phase reactions of precursor-derived ceramics of the Si–C–N and the Si–B–C–N systems at temperatures higher than 1700 K are described. CALPHAD (CALculation of PHAse Diagrams) results confirm quantitatively the data from thermogravimetry and differential thermal analysis of precursor-derived Si–C–N ceramics. A model for explanation of the thermal stability of specific Si–B–C–N precursor ceramics was developed. Phase reactions of polymeric precursors of the Si–C–N–H system were calculated and compared with analyses concerning the composition of the solid ceramic and gaseous products from thermolysis at a temperature of 1323 K. The results show that a semi-quantitative description of the thermolysis process is possible. Copyright © 2001 John Wiley & Sons, Ltd.

Keywords: phase equilibria; Si–B–C–N ceramics; thermolysis; Calphad

Received 15 April 2000; accepted 12 September 2000

1 INTRODUCTION

Ceramics on the basis of elements such as silicon, boron, carbon and nitrogen are of special interest owing to the strong covalent bonds in their structure. A special feature of such structures is the low atomic mobility, providing an outstanding microstructure stability even at very high temperatures. These materials are conventionally prepared by powder technology with sintering additives for densification.[1,2] In most cases these additives form oxidic-type secondary phases with increased atomic mobility, which substantially degrade the thermal, chemical and mechanical high-temperature stability.

In order to make use of the real high-temperature properties of covalent ceramics, alternative synthesis routes are of interest. In this context the process of thermolysis of element–organic polymers has attracted great interest in recent years because it is both scientifically and technically unique:[3–8] scientifically, because the atomic structure and microstructure of materials produced by this process can be designed to some extent by the molecular composition of the starting materials; technically, because novel materials with attractive properties can be processed in a comparatively uncomplicated manner at relatively low temperatures. The innovative idea of this procedure is that the atomic structure of the inorganic materials is closely related to the structural units of the starting polymers. In the first step, by means of standard or ingenious new methods, polymer precursors with tailored molecular structure, varying compositions and homogeneous elemental distributions on the atomic scale are produced; these are transformed in a second step by thermolysis, a well-defined heat treatment ($T = 1323$ K), into purely inorganic materials.

After thermolysis, these materials are normally amorphous and atomically homogeneous. Such materials were found to have a short-range ordered atomic structure originating from the polymer structure.[8] Since these materials are metastable they represent a starting material to be crystallized during further heat treatments at elevated temperatures into phases thermodynamically stable at a given chemical composition. Microstructures with even nanocrystalline features can be developed by controlling nucleation and grain growth. In view of

* Correspondence to: H. J. Seifert, Max-Planck-Institut für Metallforschung und Institut für Nichtmetallische Anorganische Materialien, Universität Stuttgart, Pulvermetallurgisches Laboratorium, Heisenbergstraße 5, D-70569, Stuttgart, Germany.
Contract/grant sponsor: Deutsche Forschungsgemeinschaft.
Contract/grant sponsor: Japan Science and Technology Corporation.

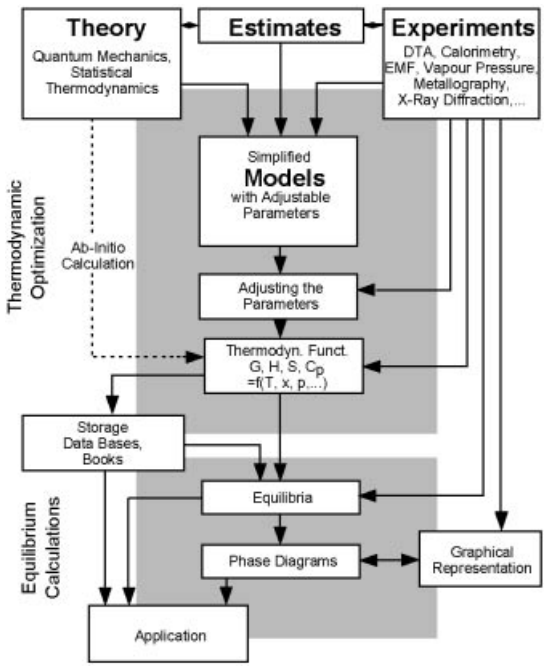

Figure 1 Scheme of the CALPHAD method.[16].

this, the phase equilibria of the ternary system Si–C–N and the quaternary system Si–B–C–N are of great interest.

To simulate and predict the phase equilibria and phase reactions in ceramics of the Si–B–C–N system, thermodynamic calculations using the CALPHAD (CALculation of PHAse Diagrams[9]) method have been carried out[10–15, 33] and these are reviewed here. Additionally, new data are presented and the possibilities of equilibrium calculations to understand the thermolysis of element–organic polymers of the Si–C–N–H system are outlined.

2 THERMODYNAMIC CALCULATIONS

Thermodynamic calculations require software packages to calculate the materials phase equilibria, phase reactions and accompanying microstructure development. The basis for these calculations is reliable thermodynamic datasets with analytical descriptions of the Gibbs energy for all phases of the system.

2.1 The CALPHAD approach

The CALPHAD method[9] is used to facilitate calculation of phase equilibria, phase reactions and thermodynamic functions of multicomponent systems under physico-chemical conditions not previously subjected to experimental investigations. A scheme of the method is shown in Fig. 1.[16] Receiving reliable results from extrapolating calculations requires self-consistent descriptions of all thermodynamic functions of state. Therefore, analytical formulae have to be provided describing the Gibbs energies for all stable phases and gas species of the particular system. In the course of the so-called 'thermodynamic optimization', model parameters are adjusted to various types of experimental data (phase diagrams and thermodynamics), using the least squares method after Gauss. In the case of incomplete experimental data, estimates and *ab initio* data can be taken into account. The thermodynamic data are stored in a computer database and binary and ternary system descriptions can then be combined to extrapolate to multicomponent phase diagrams. Well-established CALPHAD software packages are available and have been used in this work, such as BINGSS/BINFKT[17] and THERMO-CALC.[18] For the success of the CALPHAD method, when applied to a practical problem it is crucial that the most appropriate diagrams for the particular case being considered are calculated. In this work different types of phase diagram (isothermal sections, temperature–composition sections, potential diagrams), phase fraction and phase composition diagrams are used to simulate and understand phase reactions and crystallization behaviour of precursor-derived Si–(B–)C–N ceramics and the decomposition reactions of element–organic polymers containing silicon, carbon, nitrogen and hydrogen. Analytical descriptions for all phases of the Si–B–C–N and Si–C–N–H systems were developed in this work or taken from the Scientific Group Thermodata Europe (SGTE) database.[19]

2.2 Thermodynamic data

2.2.1 The Si–B–C–N system

The unary phase data for the pure elements and the descriptions for the gaseous species (e.g. N_2, Si, Si_2, Si_3, SiN, Si_2N, Si_2C, SiC_2, CN, C_2N_2) were taken from the SGTE substance database.[19] Datasets for the binary Si–B, Si–C, B–C and B–N systems were thermodynamically optimized within the scope of our work on the quaternary Si–B–C–N

Table 1 Chemical compositions (at.%) of the PNVS- (VT50-), PHMC-, PMVC-, PHMS- (NCP200) and PMVS-derived amorphous ceramics

Polymer	Si	C	N
PNVS (VT50)	26.1	39.0	34.9
PHMC	24.8	40.4	34.8
PMVC	26.3	43.3	30.4
PHMS (NCP200)	40.1	23.0	36.9
PMVS	27.6	44.8	27.6

system.[10,20] The description for the binary system Si–N was taken from the literature.[21] The liquid phases and the solid phases silicon, β-boron, graphite, SiC, Si_3N_4, $B_{4+\delta}C$, α-BN, B_3Si, B_6Si, and B_nSi were taken into account. Because of only small energetic differences, single analytical Gibbs-energy descriptions were used to describe α- and β-SiC and α- and β-Si_3N_4. α-Si_3N_4 is generally accepted to be a metastable phase.[22] The only phase with a significant homogeneity range is $B_{4+\delta}C$, which was modelled in close orientation to the crystal structure. The postulated compound C_3N_4[23] was not found as a solid phase until now.

The ternary system Si–B–C was optimized in the scope of our work on the Si–B–C–N system.[10] The other three ternary systems (Si–B–N, Si–C–N, B–C–N) could be calculated comprehensively by thermodynamic extrapolation. The ternary phases SiC_2N_4 and Si_2CN_4 reported by Riedel *et al.*[24] are not stable under the conditions treated here. Comparison with experimental data shows that adjustment of ternary parameters is not necessary. The ternary descriptions were combined in a database to simulate the phase equilibria in the quaternary Si–B–C–N system.

2.2.2 The Si–C–N–H system

For this system the thermodynamic description for the phases and gaseous species of the Si–C–N system as described above has been applied, together with the thermodynamic descriptions for the hydrogen-containing gaseous species (e.g. H_2, CH_4, NH_3) included in the SGTE database.[19] No hydrogen-containing stable solid compounds are known in the Si–C–N–H system and, therefore, it was possible to calculate it by extrapolation.

3 EXPERIMENTAL PROCEDURE

Amorphous Si–C–N ceramics were derived from commercially available precursor polyhydridomethylsilazane (PHMS (NCP200); Nichimen Corp., Tokyo, Japan; composition see Table 1) as described in detail elsewhere.[25] The polysilazane was crosslinked at a temperature of 673 K in vacuum and in argon atmosphere, and then thermolysed at 1323 K in an argon atmosphere into the amorphous ceramics. The products were ball milled to powders with an average grain size of 10 μm. Differential thermal analysis (DTA) and thermogravimetry (TG) were carried out simultaneously in a nitrogen atmosphere and BN crucibles (simultaneous thermal analysis (STA); Bähr STA501 with graphite heating element). The heating rate was 10 K min^{-1} up to 1273 K, and 5 K min^{-1} up to the maximum temperature of 2273 K.[15]

4 PHASE REACTIONS IN THE Si–C–N SYSTEM

Precursor-derived Si–C–N ceramics are X-ray amorphous after thermolysis but start to crystallize at temperatures of about 1700 K. Thermodynamic calculations, as presented in this work, are valid for determination of phase equilibria of crystalline phases. Therefore, the results can be used for explanation of phase reactions of precursor-derived ceramics at temperatures higher than about 1700 K.

Typical compositions of five precursor-derived ceramics (derived from polysilazanes and carbodiimides) are shown in Table 1. The production of these ceramics by thermolysis is described in detail in Ref 26. The compositions of the corresponding preceramic polymers are given in Table 3 (see Section 6).

4.1 Thermodynamic calculations

Figure 2 shows calculated phase equilibria of isothermal, isobaric ($p = 1$ bar) sections in the ternary system Si–C–N for the temperatures $1687 < T < 1757$ K (Fig. 2a), $1757 < T < 2114$ K (Fig. 2b) and $T = 2123$ K (Fig. 2c).[15] Additionally, Fig. 2a shows the compositions of as-thermolysed amorphous ceramics (see Table 1). For a PHMS-derived ceramic the reaction paths during degassing above 1757 K are indicated by arrows in Fig. 2b and c. The reaction paths[27] indicate the change of the gross composition of the solid samples due to the loss of nitrogen according to Reactions [1] (Fig. 2b) and [2] (Fig. 2c); see below.

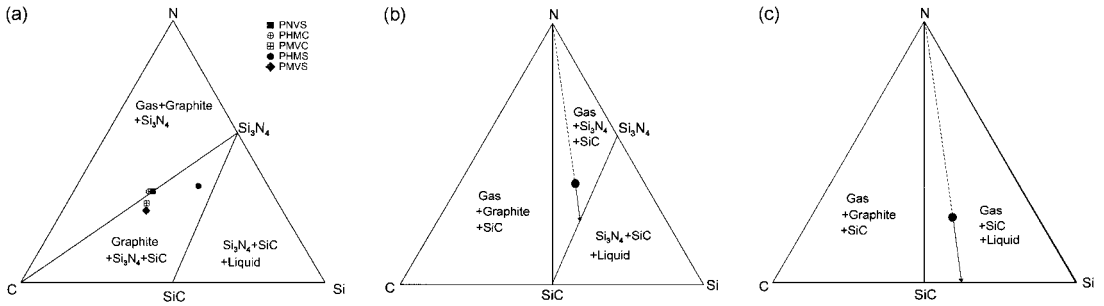

Figure 2 Isothermal, isobaric sections in the Si–C–N system at 1 bar. The compositions of amorphous precursor-derived ceramics and the reaction paths for PHMS-derived ceramic (arrows) are indicated:[15] (a) $1687 < T < 1757$ K; (b) $1757 < T < 2114$ K; (c) $T = 2123$ K.

At temperatures between 1687 and 1757 K (Fig. 2a) the following three phase fields exist: (1) gas + graphite + Si_3N_4; (2) graphite + Si_3N_4 + SiC; and (3) Si_3N_4 + SiC + liquid. The liquid phase consists of nearly pure silicon. Below 1687 K silicon exists as solid phase. The compositions of the PNVS-, PHMC- and PMVC-derived ceramics are almost located on the tie line between graphite and Si_3N_4. Under the assumption of the materials' complete crystallization, it consists of these two phases and only a very small amount of SiC.

At 1757 K and 1 bar nitrogen, Si_3N_4 and graphite react according to the invariant reaction

$$Si_3N_4(s) + 3C(s) = 3SiC(s) + 2N_2(g) \qquad [1]$$

and at temperatures between 1757 and 2114 K (Fig. 2b) the phase equilibria (1) gas + graphite + SiC, (2) gas + Si_3N_4 + SiC, and (3) Si_3N_4 + SiC + liquid exist. In connection with Reaction [1], the PHMS-derived ceramics with a ratio C:Si < 1 loses nitrogen and changes the composition towards the SiC–Si_3N_4 tie line (Fig. 2b). At temperatures above 2114 K the PHMS-derived ceramic again loses nitrogen (Fig. 2c) because the residual Si_3N_4 decomposes into liquid silicon and nitrogen gas according to the reaction

$$Si_3N_4(s) = 3Si(l) + 2N_2(g) \qquad [2]$$

The reaction path ends on the SiC–Si(l) tie line, and only two three-phase fields exist: (1) gas + graphite + SiC and (2) gas + SiC + liquid. These phase fields remain up to very high temperatures.

The influence of the gas phase on the phase Reactions [1] and [2] is shown in Fig. 3 by the calculated potential phase diagrams for C:Si < 1 (e.g. valid for PHMS ceramic).[15] The way of calculation of such diagrams is described elsewhere.[11] The gas phase is considered to be outside the system, but may exchange nitrogen with the system. Along the upper line the three phases, graphite, SiC and Si_3N_4, are in equilibrium and are subject to Reaction [1]. Below the line the two-phase field SiC + Si_3N_4 exists. Si_3N_4 decomposes at low partial pressures of nitrogen according to Reaction [2] into nitrogen and liquid or solid silicon, depending on temperature. Note the change of the reaction temperatures with the changing partial pressure of nitrogen (reaction [1]: 1757 K at 1 bar and 1973 K at 10 bar; reaction [2]: 2114 K at 1 bar and 2307 K at 10 bar). The diagram gives advice for the sintering of Si_3N_4–SiC samples. If the nitrogen partial pressure is above the line SiC + C + Si_3N_4 the sample is stable at the sintering temperature. For sintering of materials consisting of SiC and Si_3N_4 there are temperature-

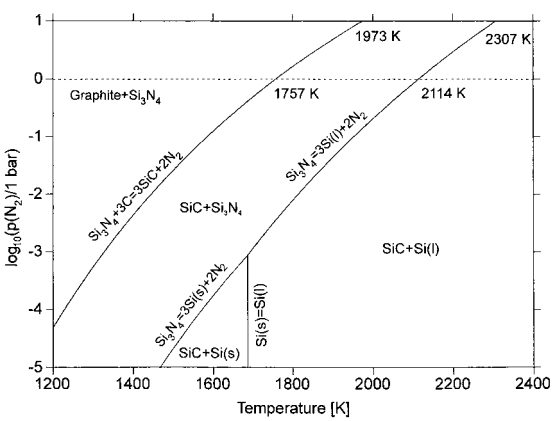

Figure 3 Potential phase diagram for the Si–C–N system valid, for example, for PHMS-derived ceramics with C:Si < 1.[11,15].

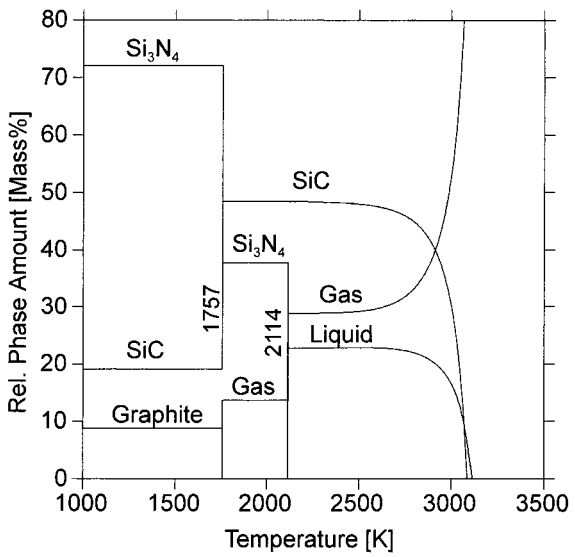

Figure 4 Calculated phase fraction diagram in the Si–C–N system for PHMS-derived ceramics (C:Si < 1).

dependent upper and lower limits for the nitrogen pressure for the stability range. During cooling from the sintering temperature for such samples the nitrogen pressure has to be lowered simultaneously to keep the sample in the SiC + Si_3N_4 phase field. For more details see Refs 11, 15, 28, 29.

Additionally, quantitative mass balances and reaction enthalpies for the ceramics can be calculated to be compared with experimental STA investigations.[14,15] For this purpose the phase fraction diagram was calculated. For a PHMS-derived ceramic (Fig. 4) with a ratio C:Si < 1 all carbon is consumed and there is a mass loss (nitrogen gas formation) of 13.7% due to Reaction [1] at 1757 K (1484 °C). The calculated enthalpy of reaction is +28.5 kJ mol^{-1}. Excess Si_3N_4 remains after the reaction (see also reaction path Fig. 2b). At a higher temperature of 2114 K (1841 °C) this residual Si_3N_4 decomposes according to Reaction [2], causing a further mass loss of 15.1% (see also reaction path Fig. 2c; enthalpy of reaction: +49.5 kJ mol^{-1}).

4.2 Experimental investigations

Figure 5 shows the DTA/TG curves for the PHMS-derived ceramic.[14,15] Two steps of mass loss with accompanied endothermic reactions were detected, as predicted by thermodynamic calculation (Figs 2b and c and 4). In the temperature range from 1600 to 1690 °C (1873–1963 K) a 12% mass loss (calculated value: 13.7%) and an endothermic reaction

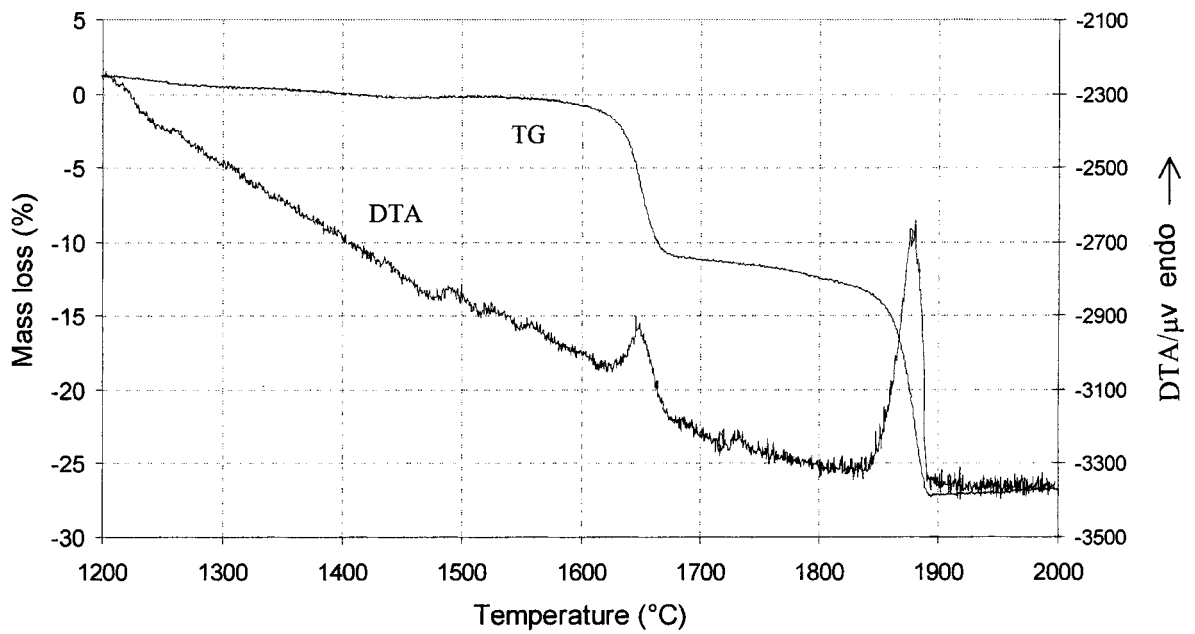

Figure 5 DTA/TG measurements (STA) of PHMS precursor-derived ceramic: nitrogen atmosphere; BN crucible; 10 K min^{-1} up to 1000 °C (1273 K); 5 K min^{-1} up to 2000 °C (2273 K).

Table 2 Chemical compositions of the PMBS(m)-, PHBS(p)- (MW33-), PHBS(m)- and PMBS(p)-derived amorphous ceramics

	Composition (at.%)			
Polymer	Si	B	C	N
PMBS(m)	28.6	9.2	41	21.2
PHBS(p) (MW33)	25.1	9.1	38.9	26.9
PHBS(m)	24.5	10	40	25.5
PMBS(p)	26.5	9.3	42.5	21.7

peak were detected, and between 1840 and 1900 °C (2113 and 2173 K) a 15% mass loss (calculated value: 15.1%) and an endothermic reaction peak were determined. The first endothermic peak can be attributed to Reaction [1], although the measured temperature is a little higher than calculated. However, it is well known that Reaction [1] is of sluggish character and the reaction temperature cannot be determined exactly by DTA/TG using heating rates of 5 K min^{-1}. Extended sample heat treatment is necessary to confirm the reaction temperature as calculated.[15] The second endothermic peak is due to the decomposition of residual Si_3N_4 according to Reaction [2]. The two steps of mass loss agree quantitatively with those calculated. The ratio of the two experimentally derived enthalpy values (the area of the endothermic peaks) is similar to the ratio of the calculated enthalpies. The temperature of Reaction [2] is in agreement with that calculated. Further analyses by X-ray diffraction (XRD), scanning electron microscopy (SEM) and energy dispersive X-ray spectroscopy (EDX) also confirmed the calculated results.[14,15]

5 PHASE REACTIONS IN THE Si–B–C–N SYSTEM

Typical compositions of four precursor-derived Si–B–C–N ceramics are shown in Table 2. All materials have a boron content of about 10 at.%. The processing of these ceramics is described in detail in Ref. 8. Phase equilibria in a quaternary system can be displayed in a concentration tetrahedron, as is shown for the Si–B–C–N system in Fig. 6. The stable solid phases in the system and a plane at a constant boron content of 10 at.% including the composition of the precursor-derived ceramic PHBS(p) (MW33) are indicated.

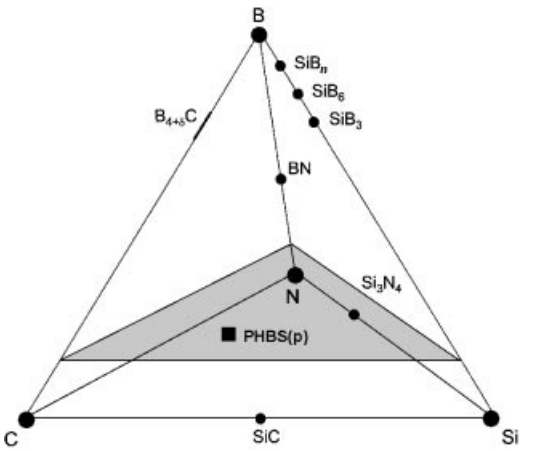

Figure 6 Si–B–C–N concentration tetrahedron with indicated plane at 10 at.% boron and composition of precursor-derived ceramic PHBS(p) (MW33).

Clear information on phase equilibria in the Si–B–C–N system at constant temperatures were derived from calculated quaternary isothermal sections. The isothermal sections at 1673 K and 2273 K are shown in Fig. 7a and b respectively. In both cases the (regular) concentration tetrahedron is divided into different distorted tetrahedra indicating the four-phase equilibria at the specific temperature. Concentration sections through the 1673 K and 2273 K tetrahedra at 10 at.% boron (see Figs 6 and 7a and b) were calculated and are shown in Fig. 8a and b respectively. In these sections the four-phase equilibria nos 1–6 as shown in Fig. 7a and nos 1–3 as shown in Fig. 7b appear as triangles and squares respectively, depending on the way the tetrahedra are cut. The compositions of high-temperature ($T > 2273$ K) stable precursor-derived Si–B–C–N ceramics PMBS(m), PHBS(p), PHBS(m), PMBS(p) are indicated (all with boron contents of about 10 at.%; see Table 2). At $T = 1673$ K (Figs 7a and 8a) they are all located in the phase field $Si_3N_4 + SiC + C + BN$. This phase equilibrium remains stable as low as room temperature. However, at high temperatures (e.g. 2273 K, Figs 7b and 8b) the compositions are located in the phase field $Gas + SiC + C + BN$, and some decomposition is expected. Further calculated sections with indicated precursor compositions are discussed in Ref. 8.

To find out at which temperature the decomposition reaction mentioned occurs, the phase fraction diagram for the composition of high-temperature

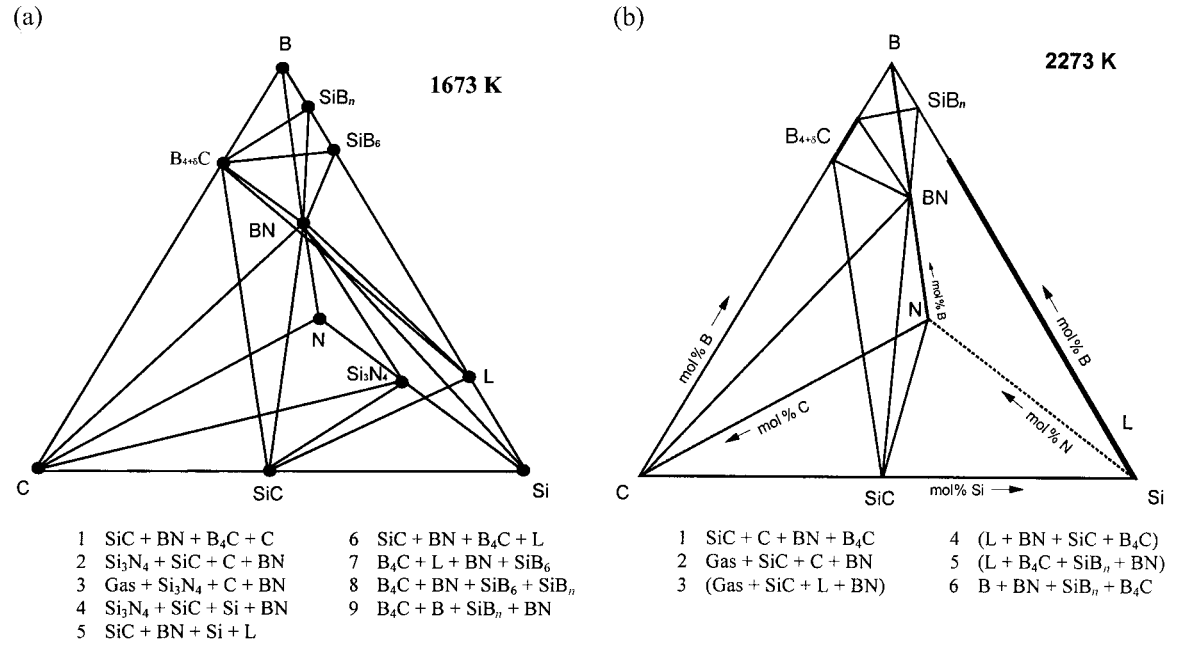

Figure 7 Isothermal sections in the Si–B–C–N system: (a) $T = 1673$ K; (b) $T = 2273$ K; for reasons of clarity only three four-phase equilibria (nos 1, 2 and 6) are shown.

stable PHBS(p)-derived ceramic was calculated and is shown in Fig. 9. As in the case for the PHMS-derived Si–C–N ceramic (see Section 4.1 and Fig. 4), Reaction [1] appears at 1757 K. Si_3N_4 reacts completely with graphite to form SiC and gas phase. Excess graphite remains. The BN phase does not take part in Reaction [1] and its amount remains stable up to a temperature of 2586 K. From this result a thermal decomposition of this PHBS(p)-derived material at 1757 K with significant mass losses (nitrogen gas) is expected. However, TG analysis shows a remarkable thermal stability for

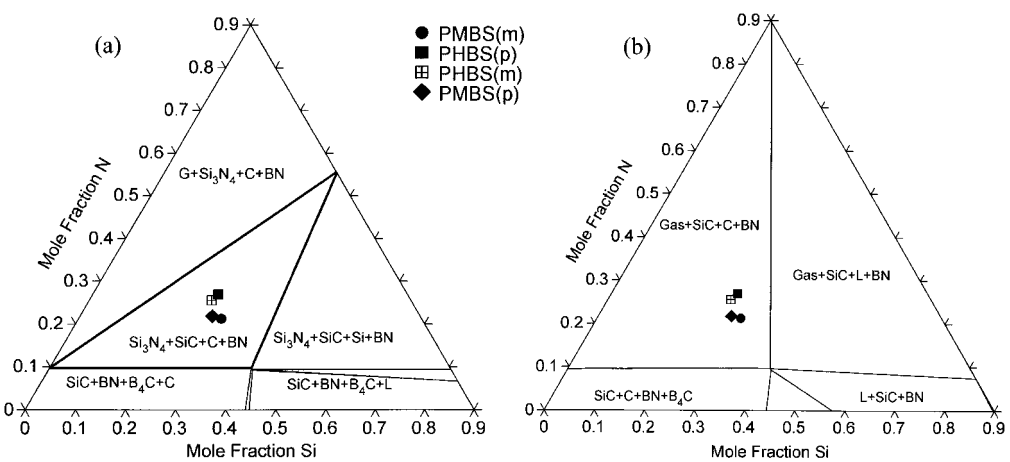

Figure 8 Concentration sections in the Si–B–C–N system at constant boron content (10 at.%) and temperatures. Phase equilibria (compare with Fig. 7) and compositions of some high-temperature stable precursor-derived ceramics are indicated (see also Table 2): (a) $T = 1673$ K; (b) $T = 2273$ K.

this material and for various other precursor-derived boron-containing ceramics up to 2300 K.[8]

To understand these conflicting results the materials' microstructure has to be taken into account. High-resolution TEM (HRTEM) reveals that the high-temperature stable materials consist of nanocrystalline Si_3N_4 grains, even in materials heat treated at temperatures higher than the decomposition temperature of Si_3N_4 (2114 K). These grains and those of SiC are embedded in a matrix of turbostratic B–N–C layers (Fig. 10[30]). Analyses of such B–N–C layers in PHBS(p)-derived ceramics with electron spectroscopic imaging (ESI) show a B:N:C ratio of 1:1:3.3.[8] The calculated B:N:C ratio can be derived from the (BN + C) fraction in Fig. 9. The boron and nitrogen amounts are both 9 at.% (note the mole of atoms units); the graphite fraction is 28 at.%. This result is in very good accordance with the experimentally derived ratio.

Looking at the microstructure of the high-temperature stable precursor-derived Si–B–C–N ceramics, an 'encapsulation effect' has been assumed[11] that results in a diffusion barrier for nitrogen, a correlated internal pressure increase and an accomponied silicon nitride stabilization. To understand the effect of increased pressure on the decomposition and reaction temperatures of Si_3N_4, calculated potential phase diagrams can be used (Figs 3 and 11). In these diagrams the phase equilibria dependence on the partial pressure of nitrogen and temperature are shown. Details of the calculation of such diagrams for Si–B–C–N materials are described in Ref 11. Figure 3 shows that the Si_3N_4 decomposition temperature, according to Reaction [2], increases from 2114 K at a total pressure of 1 bar to a temperature of 2307 K for a total pressure of 10 bar. Another potential phase diagram was calculated for PHBS(p) precursor-derived ceramics (Fig. 11). To calculate this diagram the Si:B:C ratio with regard to the PHBS(p)-derived material was fixed with $Si_{33}B_{13}C_{54}$ and the nitrogen potential was varied. Along the upper line, Si_3N_4, SiC and graphite are in equilibrium with the gas phase. When crossing this line, one of the phases disappears according to Reaction [1]. Above the line the solid phases graphite, Si_3N_4 and BN are in equilibrium with the gas phase, whereas below the line graphite, SiC and BN are in equilibrium with the gas phase. For the given $Si_{33}B_{13}C_{54}$ composition some excess graphite remains after the complete consumption of Si_3N_4. Increasing the nitrogen pressure from $p_{N_2} = 1$ bar to 10 bar the temperature of Reaction [1] is increased from 1757 to 1973 K, which also

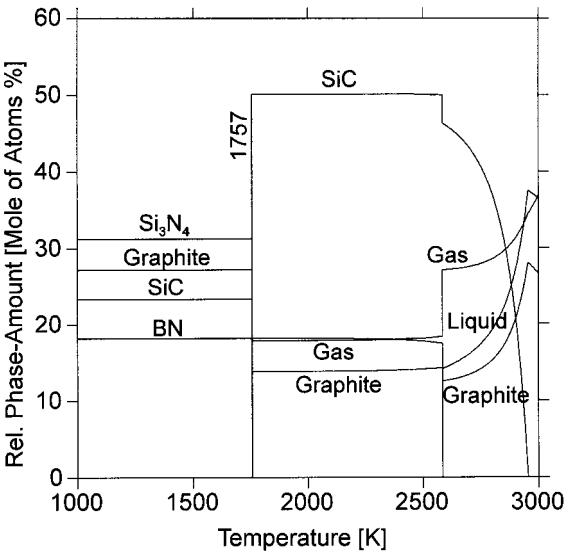

Figure 9 Phase fraction diagram for composition of Si–B–C–N ceramics derived from PHBS(p) precursor.

indicates a stabilization of Si_3N_4. The potential phase diagrams for other precursor ceramics are shown in Ref 11.

A further effect increasing the reaction tempera-

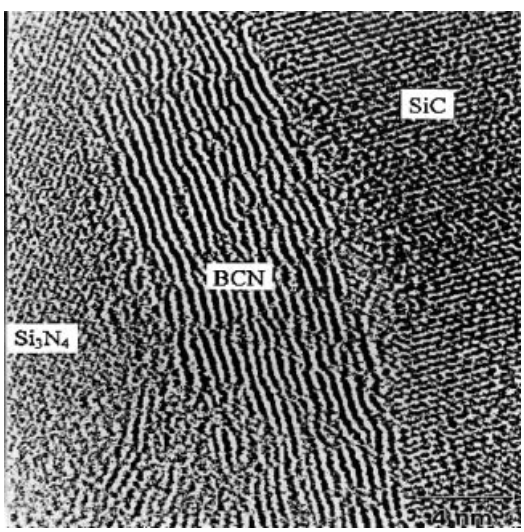

Figure 10 HRTEM image of Si–B–C–N ceramics showing an SiC and an Si_3N_4 grain and turbostratic B–N–C layers. Reprinted from *Composites Part A*, **27A**, A. Jalowiecki, J. Bill, F. Aldinger, J. Mayer, 'Interface characterization of nanosized B-doped Si_3N_4/SiC ceramics', page 721, Copyright 1996, with permission from Elsevier Science.[30]

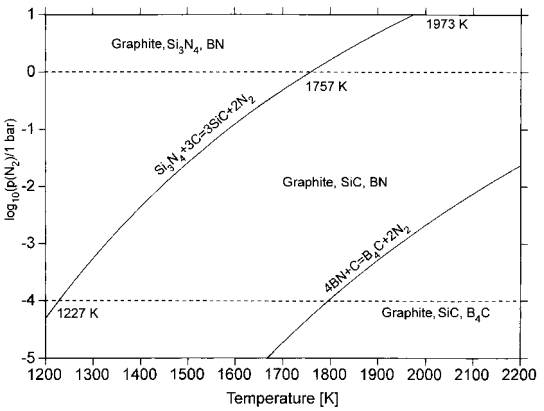

Figure 11 Calculated $\log(p_{N_2})$–temperature diagram for $Si_{33}B_{13}C_{54}$ composition.

ture of Reaction [1] is due to the dissolution of carbon in the turbostratic B–N–C layers (Fig. 10). Consequently, the activity of carbon is decreased. Calculated activity versus temperature diagrams quantify this effect on phase equilibria, as shown in Fig. 12. At a pressure of 1 bar the reaction [1] temperature is increased from 1757 K at an activity $a_C = 1$ to 2114 K at an activity of $a_C = 0.1$. At lower carbon activities Si_3N_4 decomposes according to Reaction [2], as indicated by the horizontal line. At an assumed pressure of 10 bar the reaction [1] temperature is 1973 K and this increases to 2307 K at $a_C = 0.17$. At lower activities, again Reaction [2]

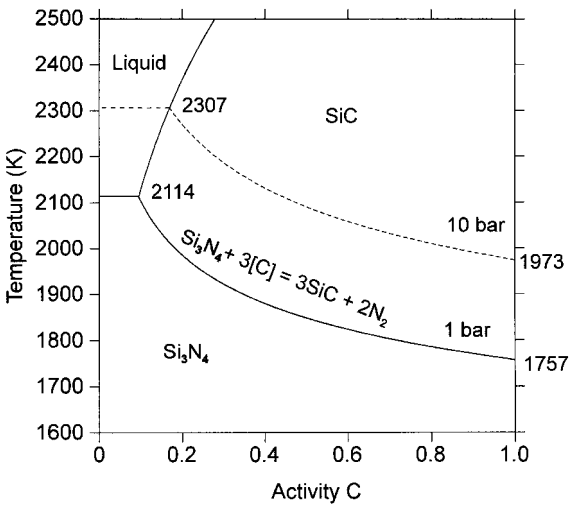

Figure 12 Temperature–activity (a_C) diagram in the Si–C–N system.

occurs. The calculated reaction temperatures are consistent with the values given in Figs 3, 4 and 11, and make clear the relationship between the different types of diagram.

These results explain the increase of temperatures for reactions with Si_3N_4 participation and explain the high-temperature stability of precursor-derived Si–B–C–N ceramics. However, it has to be emphasized that the actual pressure and activities in the Si–B–C–N ceramics are not known exactly (the pressure of 10 bar for the calculations was chosen rather arbitrarily), but the potential diagrams can show quantitatively the effects and tendencies of materials behaviour. The phase stabilities and reactions in the nanocrystalline materials may also be influenced by interface energies between Si_3N_4 or SiC grains and the B–N–C matrix. Further investigations are necessary to quantify such effects.

6 PHASE REACTIONS IN THE Si–C–N–H SYSTEM

To understand the thermolysis, phase equilibrium calculations in the Si–C–N–H system were carried out. They were made for a closed system under the assumption of complete crystallization of the phases, whereas the precursors and the resulting ceramics are amorphous and synthesized in an open system. Nevertheless, important information can be derived from such calculations. Earlier calculations in this system, but for different physico-chemical conditions, were presented in Refs 31, 32.

The thermolysis of five different preceramic polymers was investigated experimentally.[8] The compositions of these samples determined by chemical analysis are shown in Table 3. The compositions of the amorphous ceramics derived from these polymers after thermolysis are given in

Table 3 Chemical composition of preceramic polymers

	Composition (at.%)			
Polymer	Si	C	N	H
PNVS (VT50)	11.1	23.1	16.2	49.6
PHMC	8.3	24.8	16.5	50.4
PMVC	6.4	29.6	15.2	48.8
PHMS (NCP200)	11.5	15.7	10.5	62.3
PMVS	8.8	25.5	8.8	56.9

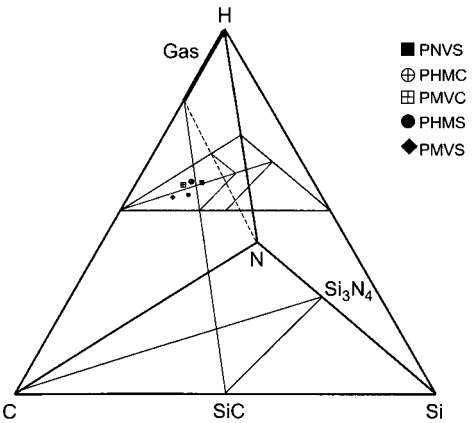

Figure 13 Si–C–N–H concentration tetrahedron. The compositions of the precursors PNVS, PHMC, PMVC, PHMS and PMVS are indicated (exact data are given in Table 3).

Table 1. The hydrogen content of all these materials is in the range of 48.8 to 62.3 at.%. For simplicity, the compositions of the precursors are displayed in the quaternary Si–C–N–H concentration tetrahedron in a plane at 50 at.% hydrogen. This plane is indicated in Fig. 13, together with the phase equilibria at 573 K.

This isothermal section at constant hydrogen content of 50 at.% and the compositions of the precursor polymers are also shown in detail in Fig. 14a. The extensions of the phase equilibrium fields change with temperature. This effect is shown in Fig. 14b, where the isothermal phase equilibria at 773, 973 and 1323 K are drawn into one section. At 773 K, and below, methane is the main gaseous species. At higher temperatures methane decomposes. At 1323 K (temperature of thermolysis) it is almost completely decomposed, and hydrogen is the dominating gas species. Therefore, the wide extensions of the phase fields $Gas + Si_3N_4$ and $Gas + Si_3N_4 + SiC$ with increasing temperature narrow to simple lines.

The polymers investigated can be separated into two classes. The compositions of PNVS, PHMC and PMVC with a ratio [Si]:[N] < 0.75 are found to be in the three-phase field $Gas + C + Si_3N_4$, whereas the compositions corresponding to the precursors PHMS and PMVS (with the ratio [Si]:[N] > 0.75) are located in the four-phase field $Gas + C + Si_3N_4 + SiC$ (Fig. 14a). The phase formation in the temperature range between 298 and 1400 K is illustrated by the solid-phase fraction diagrams (Fig. 15a) and gas-phase composition diagrams (Fig. 15b), which have been calculated thermodynamically based on the precursor compositions as given in Table 3.

In all cases the amount of CH_4 decreases with increasing temperature by continuous decomposition to form hydrogen (Fig. 15b) and graphite (Fig. 15a). However, there are also differences between the two classes of precursors mentioned regarding solid and gaseous phase formation. Precursor compositions located in the three-phase field

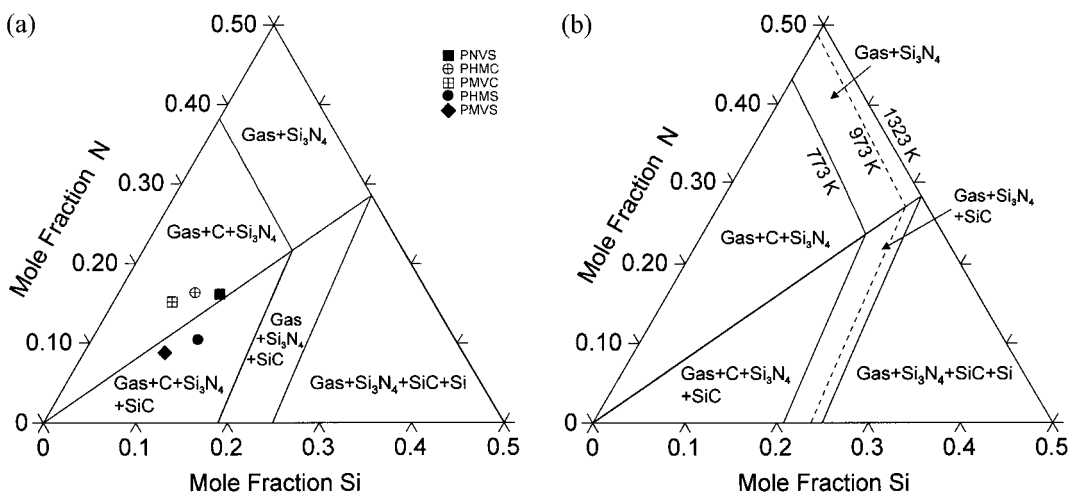

Figure 14 Isothermal sections at 50 at.% hydrogen in the Si–C–N–H system: (a) $T = 573$ K (compositions of different precursors indicated); (b) $T = 773$, 973 and 1323 K.

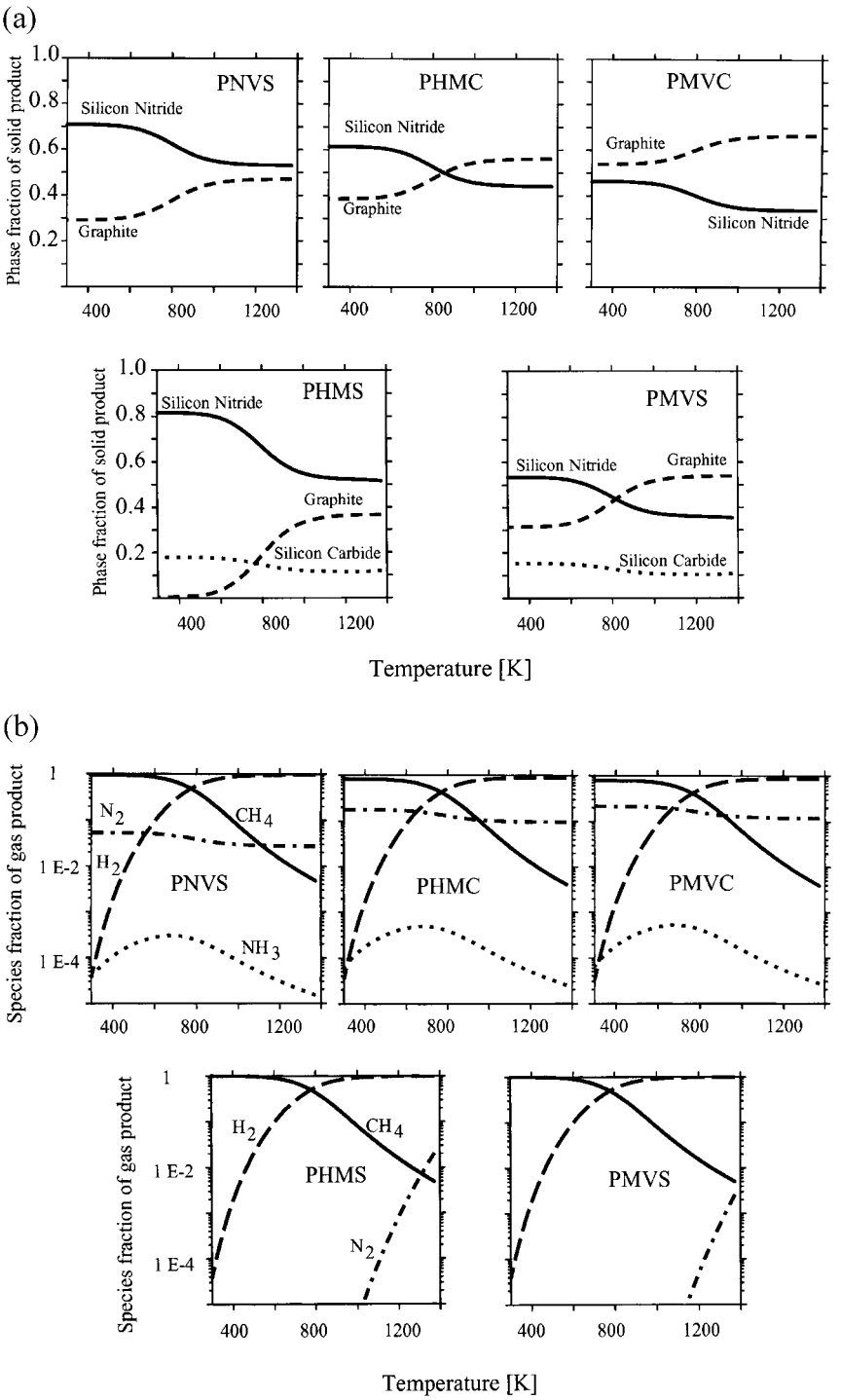

Figure 15 Results of thermodynamic calculations with precursor compositions as given in Table 3: (a) phase fractions of the solid products; (b) gas-phase compositions.

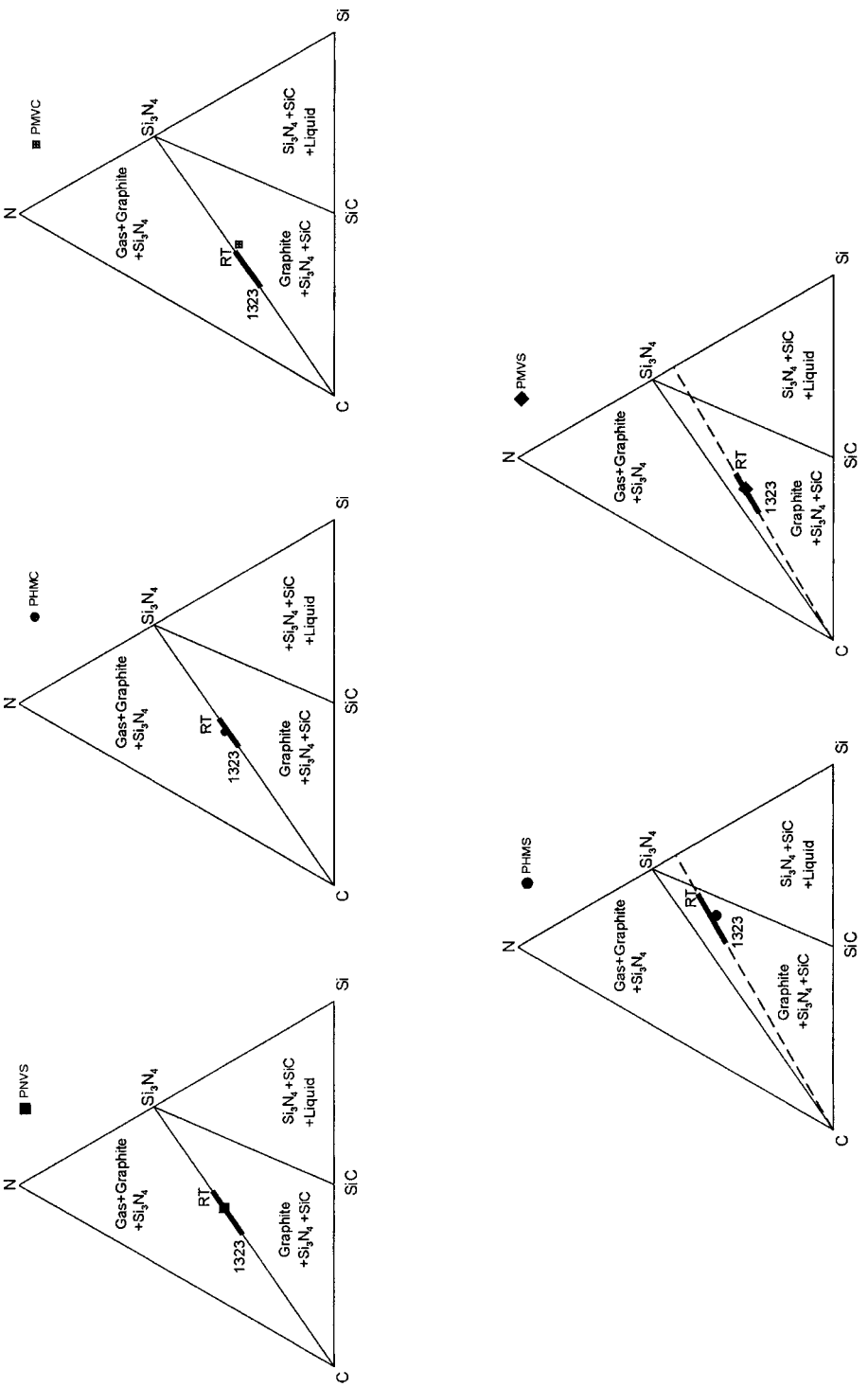

Figure 16 Compositions of solid products of precursor thermolysis calculated for temperatures between 298 (RT) and 1323 K displayed together with phase equilibria of the Si–C–N system (valid for $1687 < T < 1757$ K). The experimentally determined compositions for the ceramic products derived are indicated (as in Fig. 2a).

Gas + C + Si_3N_4 (precursors PNVS, PHMC and PMVC) yield only Si_3N_4 and graphite as solid phases (Fig. 15a). In these cases some silicon deficit with respect to the atomic ratio [Si]:[N] = 0.75 allows the formation of nitrogen-containing gas species (N_2, NH_3) (Fig. 15b) until, in the solid product, the ratio [Si]:[N] = 0.75 is reached. If the PHMS- and PMVS-derived compositions located in the four-phase field Gas + C + Si_3N_4 + SiC are considered, some excess silicon with respect to the atomic ratio [Si]:[N] = 0.75 is present. In this case the formation of SiC in addition to Si_3N_4 and carbon (graphite) is observed (Fig. 15a), and nitrogen occurs at elevated temperatures (Fig. 15b).

According to these results, after complete thermolysis the compositions of the ceramics corresponding to both classes of preceramic compounds described above are located within the basal Si–C–N plane of the concentration tetrahedron Si–C–N–H. In Fig. 16 the Si–C–N overall compositions of the solid *amorphous* products calculated between room temperature (RT) and 1323 K (temperature of thermolysis) are inserted as bold lines into the Si–C–N phase diagram valid for temperatures between 1687 and 1757 K (see also Fig. 2a). It has to be emphasized that these compositions are derived from the calculated phase fractions of *crystalline* silicon nitride, graphite and silicon carbide, as shown in Fig. 15a. As mentioned before, crystallization of Si–C–N precursor-derived ceramics requires temperatures higher than 1700 K. Hence, the gross composition of the amorphous ceramics is derived indirectly from the fraction of the phases appearing, on the assumption that materials crystallization occurs even at lower temperatures. However, the calculations can give an idea on the composition and short-range order in the amorphous microstructure, which is in close relation to the structure of the phases crystallizing at higher temperature.

As can be seen from the diagrams in Fig. 16, the compositions of solid products calculated in the case of the PNVS-, PHMC-, and PMVC-derived ceramics are located on the tie line Si_3N_4–C. The solid phase compositions calculated for PHMS- and PMVS-based materials are found along the concentration line (dotted lines) close to the ratio [Si]:[N] = 1 inside the tie triangle graphite–Si_3N_4–SiC. In addition, Fig. 16 also contains the experimentally derived compositions (after thermolysis at 1323 K) of the amorphous ceramic solids as given in Table 1 and already indicated in Fig. 2a. Concerning the Si:N ratios, a good correspondence between calculated and experimentally derived compositions can be seen. However, for all cases the calculated carbon contents at 1323 K are higher than the experimentally derived values. As pointed out, the calculated [Si]:[N] ratios of the solid phases remain constant within the considered temperature range, but the calculated carbon content increases with temperature as a consequence of the decreasing amount of CH_4 released in gas phase (Fig. 15a and b).

Owing to continuous loss of carbon-containing gaseous species during thermolysis (open system under flowing argon gas), the experimentally determined carbon content of the ceramic obtained is lower compared with the compositions calculated for 1323 K. However, it is not reaching the equilibrium composition at room temperature (RT, Fig. 16).

PNVS, PHMC and PMVC all yield ceramics that exhibit a [Si]:[N] ratio close to 0.75. As a result, the ratio [Si]:[N] < 0.75 determined for the polymers is increased in the corresponding ceramics. Mass spectroscopy shows a significant loss of nitrogen- and carbon-containing gaseous species (CH_4, NH_3, $(CN)_2$, N_2) during thermolysis of these polymers.[8]

Compared with the calculations presented in Fig. 15b, which reveal that, besides CH_4, mainly nitrogen is present in the gas phase, this experimental result indicates that the loss of nitrogen also involves the formation of metastable gaseous species. On the other hand, the molar ratio of silicon and nitrogen present in PHMS and PMVS is maintained within the corresponding ceramic solids, and compositions with an [Si]:[N] ratio close to one are obtained. This observation is in accordance with the results obtained by mass spectroscopy, which reveal that methane and hydrogen are the main gaseous decomposition products.[8]

It has to be emphasized that these calculations were carried out for a closed system, as described before. In contrast to this, during thermolysis a continuous loss of gaseous species and a continuous change of the gross composition of the solid material can be found, accompanied by a change in the ratio of the gaseous species involved. This results in bent reaction paths[27] due to the continuous change of the ratio of the gaseous species (mainly methane and hydrogen) starting in the 'space' of the Si–C–N–H concentration tetrahedron (Fig. 13) and ending on the tie line C–Si_3N_4 or in the tie triangle graphite–Si_3N_4–SiC of the Si–C–N system.

Owing to the loss of carbon-containing gaseous species during thermolysis, the experimentally

determined carbon content of the ceramics obtained is shifted to lower values compared with the compositions calculated for 1323 K (Fig. 16). However, spectroscopic investigations indicate that the decomposition of methane contributes to the formation of carbon during the thermolysis step. According to mass spectra, the evolution of methane is observed in the temperature range between 700 and 1000 K with a maximum intensity in a temperature range that corresponds to calculated data (Fig. 15b). Above this temperature the methane amount decreases, whereas the amount of hydrogen increases, this is accompanied by the formation of sp^2-hybridized carbon, as revealed by ^{13}C NMR spectroscopy.[8] These results suggest that the incorporation of free carbon into the ceramic solids is caused by the decomposition of methane.

In the case of the carbodiimide-based precursors, cyano compounds may also play a role during thermolysis. With PHMC, for example, $(CN)_2$ was found to be the main gaseous decomposition product.[8] In agreement with the evolution of nitrogen detected by mass spectroscopy, this observation suggests the formation of solid carbon from metastable $(CN)_2$ species to form graphite and nitrogen.

According to the above-mentioned thermochemical calculations, the compositions of the precursor-derived ceramics are located close to the tie line Si_3N_4–C (PNVS-, PHMC- and PMVC-derived ceramics) and inside the area defined by the three-phase equilibrium Si_3N_4–SiC–C (PHMS- and PMVS-derived ceramics). The structural investigations of the amorphous ceramics described in Ref. 8 also reveal that the PNVS-, PHMC-, and PMVC-derived solids consist of SiN_4 tetrahedra and sp^2-hybridized carbon units. In the case of the PHMS- and PMVS-based materials, CSi_4 and SiC_xN_y tetrahedra are present in addition to SiN_4 and sp^2-hybridized carbon units. In addition, the results on the medium-range order clearly exhibit the presence of silicon nitride segregations. The surrounding matrix is enriched in carbon in the case of the compositions located close to the tie line Si_3N_4–C, whereas the amount of silicon is increased if the composition is located inside the tie triangle graphite–Si_3N_4–SiC. These results indicate that the structural units of the thermodynamically stable phases are already preformed within the amorphous states on an atomic- and medium-range scale. Although kinetic aspects, like the formation of metastable radical and gaseous intermediate species, play an important part, thermodynamic considerations provide an important base for the correlation of the precursor composition with the architecture of the corresponding amorphous ceramic solids.

7 CONCLUSION

Thermodynamic calculations according to the CALPHAD-method can be used to track phase equilibria and phase reactions of precursor-derived ceramics and to contribute to the understanding of the process of thermolysis. Combinations of such calculations with selected experiments are the basis for an efficient materials development. Comparisons with available experimental results show that in the quaternary systems Si–B–C–N and Si–C–N–H the calculations are reliable. Based on a consistent thermodynamic dataset, the most practically useful types of phase diagram (isothermal sections, temperature–composition diagrams), phase composition diagrams and property diagrams (e.g. phase fraction diagrams) can be calculated. The results are valid to find guidelines for favourable sintering and processing conditions and the understanding of the materials' high-temperature reactions during application.

However, to use thermodynamically calculated results for the interpretation requires the consideration of the materials' microstructure, specific crystallization behaviour and the kinetics of phase formation and phase reaction. This is especially true for the interpretation of dynamical thermal analysis experiments (e.g. DTA, TG). Moreover, heat treatments (e.g. thermolysis) are often carried out in an inert atmosphere, and evaporating gaseous species are continuously removed by flowing gas atmospheres (inert or reactive). This effect greatly influences the phase reactions. Therefore, thermodynamic calculations for the simulation of such processes are in progress.

Acknowledgements We thank the Deutsche Forschungsgemeinschaft (DFG) and the Japan Science and Technology Corporation (JST) for financial support. We are also grateful to J. Bill, P. Gerstel, S. Prinz and J. Seitz for providing samples.

REFERENCES

1. Lange FF. *Am. Ceram. Soc. Bull.* 1983; **62**: 1369.
2. Greil P, Petzow G and Tanaka H. *Ceram. Int.* 1987; **13**: 19.

3. Birot M, Pillot J-P and Dunogués J. *Chem. Rev.* 1995; **95**: 1443.
4. Bill J and Aldinger F. *Adv. Mater.* 1995; **7**: 775.
5. Baldus H-P and Jansen M. *Angew. Chem.* 1997; **109**: 338.
6. Laine RM and Sellinger A. Si-containing ceramic precursors. In *The Chemistry of Organic Silicon Compounds*, vol. 2, Rappoport Z, Apeloig Y (eds). J. Wiley & Sons Ltd: London, 1998; 2245–2310.
7. Aldinger F, Weinmann M and Bill J. *Pure Appl. Chem.* 1998; **70**: 439.
8. Bill J, Kamphowe TW, Müller A, Wichmann T, Zern A, Weinmann M, Schuhmacher J, Müller K, Peng J, Seifert HJ and Aldinger F. *Appl. Organomet. Chem.* 2001; this issue.
9. Saunders N and Miodownik P. *CALPHAD (calculation of phase diagrams): a comprehensive guide*. In *Materials Series*, vol. 1, Cahn RW (ed.). Pergamon: Oxford, 1998.
10. Kasper B, Seifert HJ, Kußmaul A, Lukas HL and Aldinger F. Entwicklung eines thermodynamischen Datensatzes für das System B–C–N–Si–O. In *Proc. Werkstoffwoche '96, Stuttgart, Symp. 7, Materialwissenschaftliche Grundlagen*, Aldinger F, Mughrabi H (eds). DGM-Informationsgesellschaft mbH: Frankfurt, 1997; 623–628.
11. Seifert HJ, Lukas HL and Aldinger F. *Ber. Bunsenges. Phys. Chem.* 1998; **9**: 1309.
12. Seifert HJ, Peng J and Aldinger F. Die Konstitution von Si–B–C–N Keramiken. In *Proc. Werkstoffwoche '98, München*, Vol. VII, *Keramik/Simulation Keramik*, Heinrich J, Ziegler G, Hermel W, Riedel H (eds). Wiley–VCH: Weinheim, 1999; 339–343.
13. Seifert HJ and Aldinger F. Thermodynamic calculations in the system Si–B–C–N–O. In *Precursor-Derived Ceramics*, Bill J, Wakai F, Aldinger F (eds). Wiley–VCH: Weinheim, 1999; 165–174.
14. Peng J, Seifert HJ and Aldinger F. Thermal analysis of Si–C–N ceramics derived from polysilazanes. In *Ceramics — Processing, Reliability, Tribology and Wear, Proc. EUROMAT '99*, vol. 12, Müller G (ed.). Wiley–VCH: Weinheim, 2000; 120–126.
15. Seifert HJ, Peng J, Lukas HL and Aldinger F. *J. Alloys Compds.* 2001; **320**: 251.
16. Seifert HJ and Aldinger F. *Z. Metallkd.* 1996; **87**: 841.
17. Lukas HL and Fries SG. *J. Phase Equilibria* 1992; **13**: 532.
18. Sundman B, Jansson B and Anderson JO. *Calphad* 1985; **9**: 153.
19. Scientific Group Thermodata Europe, Grenoble Campus, 1001 Avenue Centrale, BP66, F-38402 Saint Martin D'Heres, France, http://www.sgte.org.
20. Gröbner J, Lukas HL and Aldinger F. *Calphad* 1996; **20**: 247.
21. Hillert M, Jonsson S and Sundman B. *Z. Metallkd.* 1992; **83**: 648.
22. Liang J-J, Topor L, Navrotsky A and Mitomo A. *J. Mater. Res.* 1999; **14**: 1959.
23. Fang PH. *J. Mater. Sci. Lett.* 1995; **14**: 536.
24. Riedel R, Greiner A, Miehe G, Dressler W, Fuess H and Bill J. *Angew. Chem.* 1997; **109**: 657.
25. Seitz J and Bill J. *J. Mater. Sci. Lett.* 1996; **15**: 391.
26. Bill J, Schuhmacher J, Müller K, Schempp S, Seitz J, Dürr J, Lamparter HP, Golczewski J, Peng J, Seifert HJ and Aldinger F. *Z. Metallkd.* 2000; **91**: 335.
27. Seifert HJ. *Z. Metallkd.* 1999; **90**: 1016.
28. Nickel KG, Hoffmann MJ, Greil P and Petzow G. *Adv. Ceram. Mater.* 1988; **3**(6): 557.
29. Misra AK. *J. Mater. Sci.* 1991; **26**: 6591.
30. Jalowiecki A, Bill J, Aldinger F and Mayer J. *Composites Part A* 1996; **27**: 717.
31. Gauckler L, Hucke E, Lukas HL and Petzow G. *J. Mater. Sci. Lett.* 1979; **14**: 1513.
32. Palcevskis EA, Grabis J and Miller T. *Latvijas PSR Zinatnu Akad. Vestis Kim. Ser.* 1980; **3**: 286.
33. Peng J, Seifert HJ and Aldinger F. Thermal stability of precursor-derived Si–(B–)C–N ceramics. In *Innovative Processing and Synthesis of Ceramics, Glasses, and Composites IV, Ceramic Transactions, vol. 115*, Bansal NP and Singh JP (eds). The American Ceramic Society: Westerville, Ohio, 2000; 251–262.

